RSC Advances

PAPER

View Article Online
View Journal | View Issue

Cite this: *RSC Adv.*, 2022, **12**, 21780

Boron doping positively enhances the catalytic activity of carbon materials for the removal of bisphenol A†

Hong Yi,[a] Xiaowei Huo,[*ab] Jinhong Gu,[a] Lei Wei,[a] Zhenping Sun,[a] Fuxiang Du,[*a] Chao Dai,[a] Xiongfei Wu,[a] Zhiguang Liu[a] and Jian Ren[a]

Boron-doped carbon materials (BCs), low-cost and environmentally friendly carbocatalysts, were prepared for the activation of persulfate (PS) for the removal of bisphenol A (BPA). Compared with B-free carbon materials (Cs), the adsorption and catalytic activity were significantly enhanced by the boron modification. Fast and efficient removal of BPA was achieved using the BCs/PS system. The BPA removal rate constant increased linearly with the adsorption capacity of BCs. Electron paramagnetic resonance (EPR) spectroscopy and radical quenching experiments indicated that the degradation mechanisms in the BCs/PS system were different from conventional radical-based oxidation pathways. On the contrary, nonradical pathways were demonstrated to dominate the oxidation processes in the removal of BPA using the BCs/PS system. Herein, a mechanism is proposed where PS is activated by the carbon material to form a reactive electron-deficient carbocatalyst ([BCs]*) complex with a high redox potential, driving a nonradical oxidation pathway to achieve BPA removal. Through experimental investigation and the use of electrochemical techniques (cyclic voltammetry, Tafel corrosion analysis and open circuit voltages), B-doped carbon materials for the activation of PS elevate the potential of the derived nonradical [BCs]* complexes, and then accelerate the BPA removal efficiency *via* an electron transfer process. Utilizing adsorption and nonradical oxidation processes, the BCs/PS system possesses great potential for the removal of BPA in practical applications such as wastewater treatment.

Received 28th April 2022
Accepted 12th July 2022

DOI: 10.1039/d2ra02703h

rsc.li/rsc-advances

1. Introduction

Bisphenol A (BPA) is an industrial chemical primarily used in the manufacture of polycarbonate plastics and epoxy resins, as well as in common consumer products such as bottles, binders, pipes and electronics.[1,2] It is found ubiquitously in the environment and may give rise to the pollution in various fields due to its endocrine disrupting properties and from human exposure *via* dietary and nondietary routes[3] causing organ damage.[4] Conventional wastewater treatment techniques are not capable of removing BPA from untreated water and thus, researchers have been developing new technologies for the reduction of these micropollutants.[5,6] Nowadays, advanced oxidation processes (AOPs), originally defined as techniques involving the generation and participation of hydroxyl radicals (˙OH, standard reduction potential of 2.8 V), are seen as effective and thorough strategies for the removal of organic contaminants due to their superior oxidation efficiencies.[7,8] In particular, peroxymonosulfate (PMS, HSO_5^-) and persulfate (PS, $S_2O_8^{2-}$) are typical oxidizing agents that have been used recently to degrade organic pollutants by various activation methods, such as heat,[9] ultrasound,[10] addition of a base,[11] ultraviolet light,[12] and the use of transition metals[13] to produce sulfate radicals ($SO_4^{\cdot-}$, standard reduction potential of 2.5–3.1 V), which are alternatives to ˙OH.

Carbon-based materials, such as reduced graphene oxide (rGO),[14,15] carbon nanotubes (CNTs),[16,17] carbon nanofibers (CNFs),[18] and nanodiamond[19,20] have been reported to be efficient for PS activation. This leads to the enhanced degradation of micropollutants without secondary pollution because this creates a material with an abundance of oxygen-containing functional groups, high electrical conductivity, large surface area and large pore volumes. Although PS, an inexpensive and efficient oxidant, can be activated *via* carbon-based materials,

[a]*China Construction Third Engineering Bureau Group Co., Ltd, Wuhan 430074, PR China. E-mail: hxwscu@126.com; dufuxiang2003@163.com*

[b]*College of Architecture & Environment, Sichuan University, Chengdu 610065, PR China*

† Electronic supplementary information (ESI) available: Texts describe the materials and reagents, experimental procedures, conventional analytical methods, EPR measurements, the methods for detection of PS concentrations, and electron transfer experiments. Tables show the intermediates detected using LC-MS and their associated *m*/*z* values, characteristics of various water matrices, and pore structure of the used BCs. Figures show TGA and DTG curves for the precursors heated under an N_2 atmosphere, XPS survey spectra, BPA removal efficiency at varying doses of BCs and Cs, BPA removal efficiency using Cs and BCs at varying initial pHs, and recycling test for the removal of BPA only with adsorption by BCs. See https://doi.org/10.1039/d2ra02703h

these materials still require multiple-step fabrication processes that use harsh treatments and have high costs.[21]

Heteroatom-doped carbon-based materials have been successfully applied for PS activation to enhance the oxygen reduction reaction (ORR) and catalytic activities toward organic micropollutant degradation *via* the modulation of charge electronic neutral fractures.[5,8,21–24] It was reported that, compared to undoped and boron-doped carbon nanoparticles, boron/fluorine dual-doped carbon nanoparticles drove the ORR through a two-electron pathway with low generation of the unstable peroxide, HO_2^-.[25] Balaji *et al.* prepared a phosphorus-doped reduced graphene oxide (P-rGO) which delivered a better ORR performance (0.75 A mg^{-1}) when compared with a commercial HiSPEC Pt/C (0.12 A mg^{-1}) catalyst.[26] Kaipannan *et al.* demonstrated that an activated carbon/ZnS (ACZS) nanocomposite electrode performed well as a supercapacitor and delivered a high specific capacitance of 241 F g^{-1} at 1 A g^{-1} current density.[27] Kang *et al.* synthesized a porous boron-bearing carbon electrocatalyst doped with Fe and nitrogen (Fe-BNC), which showed a high surface area (1300 m^2 g^{-1}) and favored a 4-electron reduction pathway for efficient ORR.[28]

Of the non-metallic heteroatoms available for doping, B atoms are able to break the basic sp^2-hybridized structure and create new active sites for PS activation.[29] Furthermore, Yang *et al.* demonstrated that, when used as a metal-free electrocatalyst, B-doped CNTs (B-CNTs) exhibited an enhancement of the oxygen reduction reaction compared with pristine CNTs.[30] Xie *et al.* prepared a porous interconnected 3D B-doped graphene aerogel (BGA) which could deliver a high capacity and showed outstanding rate capability for use in lithium–sulfur batteries.[31] Wu *et al.* synthesized a B-doped graphene material which showed good performance for *in situ* metal-free electrochemical advanced oxidation of BPA.[5] Therefore, B-doped carbon-based materials may contribute to effective AOP methods.

In this work, we prepared a B-doped carbon-based material *via* a simple hydrothermal process based on a mixture of coffee grounds, sodium bicarbonate and boric acid, which were all abundant, low-cost, and eco-friendly. The as-prepared BCs were adopted to activate PS for BPA degradation. In order to investigate the efficiency of BPA removal in the BCs/PS system, we explored the following aspects of the BCs/PS system. (i) The structural properties of the BCs as characterized using scanning electron microscopy (SEM) equipped with an energy dispersive X-ray spectrometer (EDX), Brunauer–Emmett–Teller (BET) analysis, X-ray diffraction (XRD), X-ray photoelectron spectroscopy (XPS), and Fourier-transform infrared spectroscopy (FT-IR). (ii) Elucidating the BCs/PS system mechanisms through experimental investigation and electrochemical techniques (including cyclic voltammetry (CV), Tafel corrosion analysis, and open circuit voltages). (iii) Studying the effects of some crucial parameters of the BCs/PS system with regard to BPA degradation, such as the dosage of the carbon material, initial pH and water matrices.

2. Methods and materials

2.1. Reagents and materials

Detailed information for materials and reagents are given in Text S1.†

2.2. Fabrication of carbon samples

Pre-BCs was prepared *via* a hydrothermal process as follows. 5 g of coffee grounds, 7 g of sodium bicarbonate and 2.1 g of boric acid were added to a beaker containing 300 mL of deionized (DI) water. The solution was magnetically stirred at 80 °C for 6 h. Then, the above mixture was dried at 80 °C for 12 h. Subsequently, the dried mixture was annealed at 700 °C for 2 h under a N_2 atmosphere with a heating rate of 5 °C min^{-1}. After naturally cooling to room temperature, the co-carbon sample was sequentially washed with DI water and ethanol and dried at 80 °C. Accordingly, the carbon samples were denoted as BCs. For comparison, a blank carbon sample was prepared by carbonization of 7 g of sodium bicarbonate and 5 g of coffee grounds at 700 °C, hereafter denoted as Cs.

2.3. Experimental procedures

Detailed information relating to the experimental procedures are shown in Text S2.†

2.4. Analytical methods

Conventional analytical methods are shown in Text S3.† Parameters for the EPR spin-trapping technique are shown in Text S4.† The concentrations of PS were determined using a spectrophotometric method (Text S5†). A CHI660E electrochemical workstation was used to conduct the electrochemical analysis (Text S6†).

3. Results and discussion

3.1. Catalytic performance of catalysts

As shown in Fig. 1, the removal of BPA using different carbon catalysts was conducted. It is notable that fullerene (C_{60}) could barely remove BPA. BPA was rapidly removed by the BCs/PS system within 60 min, which was more efficient than the CNTs/PS system, commercial graphene (G)/PS, multi-layer graphene (MLG)/PS and Cs/PS, with these catalysts having removal efficiencies within 60 min of 33.6%, 12.6%, 48.8% and 66.6%, respectively. The apparent rate constants (k_{obs}) for BPA removal using PS activated *via* various carbocatalysts follow the order: BCs (0.0710 min^{-1}) > Cs (0.0344 min^{-1}) > MLG (0.0342 min^{-1}) > G (0.0103 min^{-1}) > CNTs (0.0087 min^{-1}) > C_{60} (0.0000 min^{-1}) (Fig. 1(d)).

3.2. Characterization

Under a N_2 atmosphere, the thermogravimetric analysis (TGA) and differential thermogravimetry (DTG) were measured (Fig. S1†). For the coffee grounds/$NaHCO_3$ system, a sharp weight loss between 800 and 900 °C was observed. However, the

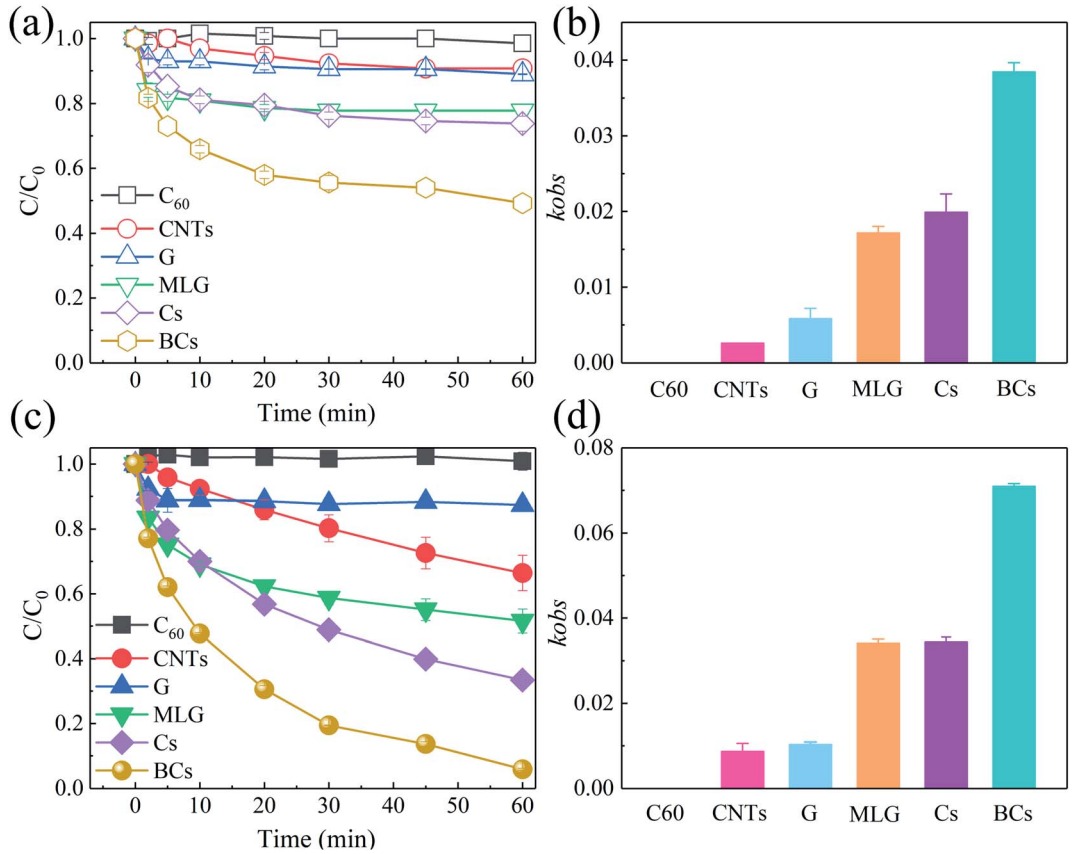

Fig. 1 BPA removal efficiency *via* adsorption of various carbon catalysts (a), and their reaction rates within 10 min (b). ($[BPA]_0 = 0.02$ mM, $T = 25 \pm 1$ °C, [carbon catalysts]$_0 = 0.1$ g L^{-1}, initial pH $= 3 \pm 0.2$). BPA removal efficiency *via* adsorption and PS oxidation of various carbon catalysts (c), and their reaction rates within 10 min (d) ($[BPA]_0 = 0.02$ mM, $T = 25 \pm 1$ °C, [carbon catalysts]$_0 = 0.1$ g L^{-1}, $[PS]_0 = 2$ mM, initial pH $= 4 \pm 0.2$).

TGA and DTG curves in the coffee grounds/$NaHCO_3$/boric acid system were different from those for the coffee grounds/$NaHCO_3$ system. The rapid weight loss in the coffee grounds/$NaHCO_3$/boric acid system only occurred at 25–150 °C, indicating that coffee grounds/$NaHCO_3$/boric acid system was more stable than the coffee grounds/$NaHCO_3$ system.

The SEM images demonstrated that the pristine Cs showed a honeycomb-like porous structure (Fig. 2(a) and (b)). Interestingly, the BCs had a coralloid-like shape after modification with boron (Fig. 2(c) and (d)). The surface pores of both the Cs and BCs were found to be mesopores. EDX elemental mapping images showed that the distribution of C, O and B elements within the carbon frameworks was uniform (Fig. 2(e)). The BET surface areas were measured using nitrogen physisorption. As illustrated in Table 1 and Fig. 3, after B doping, the specific surface area (SSA) of BCs increased from 211.712 (Cs) to 518.200 $m^2\ g^{-1}$ and the porous structures of both Cs and BCs had pore sizes mainly in the range of mesopores (2–50 nm).

The crystalline structure of Cs and BCs was studied using XRD. As shown in Fig. 4(a), the XRD patterns of Cs and BCs have a characteristic peak at 26.5° that was attributed to the (002) plane, typical plane of graphitic carbon.[32] The FT-IR spectra of BCs and Cs is shown in Fig. 4(b) and the absorption peaks at 1120, 1168, and 1397 cm^{-1} could be indexed to the vibrations of B–C stretching, B–O–H bending, and B–O stretching, respectively,[33] confirming that a large quantity of B was doped into the carbon-based materials. Additionally, the FT-IR results showed that the frameworks of BCs and Cs obtained *via* hydrothermal carbonization were similar, revealing that the B modification process did not change the structure of the carbocatalysts.

The full scan XPS spectra (Fig. S2†) showed the chemical states of carbocatalysts and that BCs contained three elements; Table 2 illustrates their elemental contents. As presented in Fig. 4(c), the B 1s spectrum provided evidence of boron oxide at 190.72 eV, interfacial suboxide boron at 187.09 eV and B–B bonds at 183.61 eV.[34] The results confirmed that boron-containing groups existed in the BCs framework. For the O 1s spectra, shown in Fig. 4(d), peaks at 533.24 and 530.64 eV were respectively assigned to C–O and C=O groups.[35] The C 1s spectra (Fig. 4(e) for BCs and Fig. 4(f) for Cs) were deconvoluted into five peaks at around 284.8, 286.1, 287.25, 288.8 and 291.1 eV, which were assigned to the sp^2-hybridized carbon bonds, C–H, C–OH or C–O–C, C=O, and O–C=O, respectively.[36]

3.3. Mechanism investigation

3.3.1. BPA adsorption kinetics and isotherms. It has been reported that the efficiency with which carbon/PS systems remove contaminants can be notably affected by the adsorptive

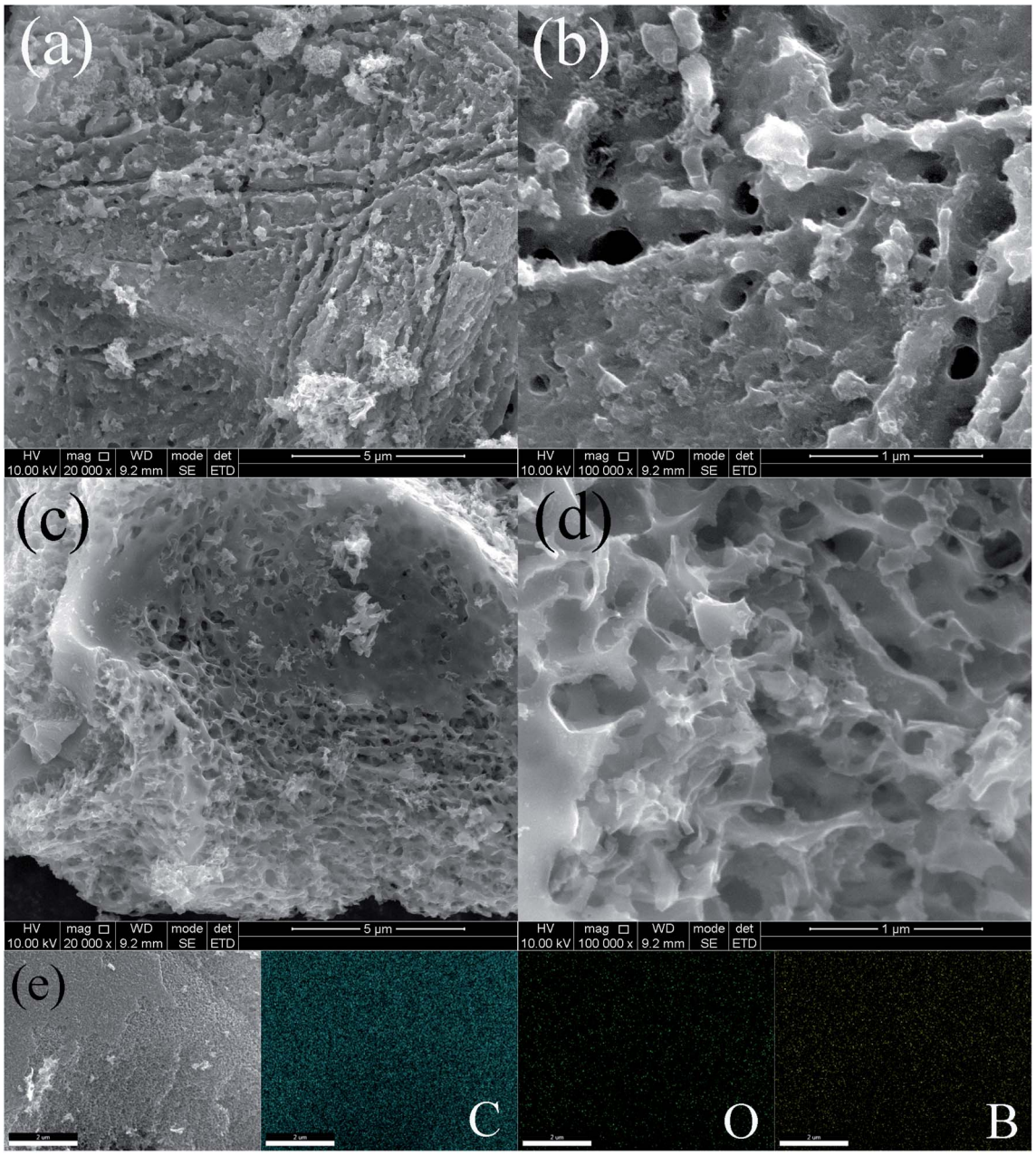

Fig. 2 SEM images of Cs (a) and (b), and BCs (c) and (d); (e) SEM image of BCs with EDX elemental mapping.

Table 1 Pore structure of Cs and BCs

Samples	BET ($m^2\ g^{-1}$)	Total pore volume ($cm^3\ g^{-1}$)	Average pore diameter (nm)
Cs	211.712	0.265	5.003
BCs	518.200	0.497	3.837

capacity of the carbocatalysts.[37,38] As shown in Fig. 5(a), when the calcination temperatures were 600, 700, 800 and 900 °C, the adsorption capacities for BPA removal after 15 min were 7.7%, 29.5%, 68.2% and 76.2%, respectively. The simultaneous use of PS and BCs showed that the removal rates for BPA were greatly enhanced to 17.2%, 55.8%, 84.8% and 82.6%, respectively. As shown in Fig. 5(c), the correlation between k_{obs} and adsorption capacities of BPA (q_e) was studied. The correlation coefficient was 0.999 for a series of BCs, indicating that the adsorption capacity was a key factor in the PS/BCs system. To further analyze the BPA adsorption by BCs and Cs, adsorption kinetics and adsorption isotherms were investigated.

The adsorption kinetics for the removal of BPA by BCs and Cs were investigated and the models were applied as follows:

Pseudo-first-order kinetic equation:[39]

$$\ln(q_e - q_t) = \ln q_e - k_1 t \quad (1)$$

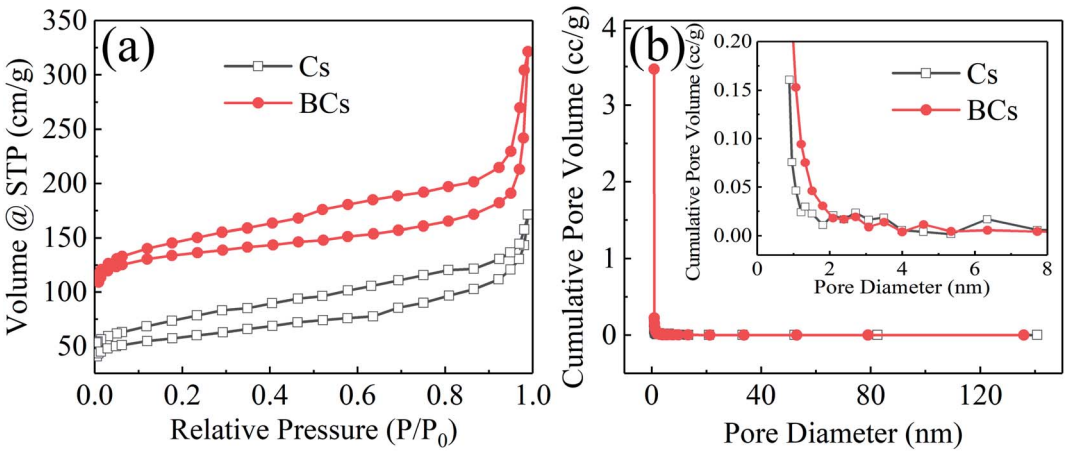

Fig. 3 (a) N_2 sorption isotherms at −196 °C; (b) Barrett–Joyner–Halenda pore-size distributions of the Cs and BCs.

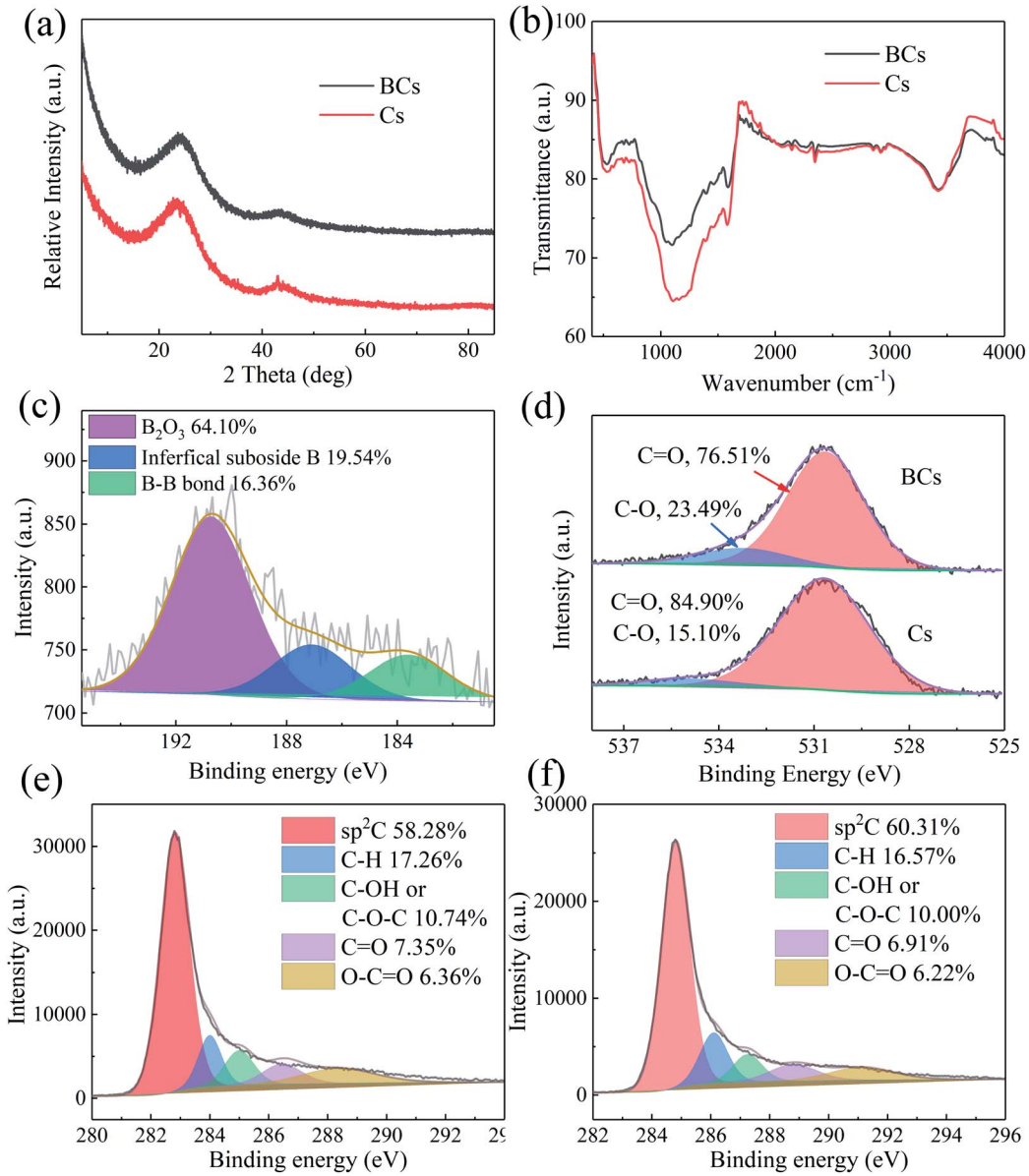

Fig. 4 XRD patterns of BCs and Cs (a); FT-IR spectra of BCs and Cs (b); B 1s high-resolution spectrum of BCs (c); high resolution O 1s spectra of BCs and Cs (d); and high resolution C 1s spectra of BCs (e) and Cs (f).

Table 2 Atomic percentages of C, O and B elements on the surface of Cs and BCs obtained from XPS analysis

Element (%)	Cs	BCs
C	89.22	89.56
O	10.78	8.36
B	—	2.08

where q_e and q_t are the adsorption capacities at equilibrium and at time t (min) in mg g^{-1}, k_1 is the rate constant of the pseudo-first-order diffusion model, g (mg min)$^{-1}$;

Pseudo-second-order kinetic model:[40]

$$\frac{t}{q_t} = \frac{1}{k_2 q_e^2} + \frac{t}{q_e} \quad (2)$$

where k_2 is the rate constant of the pseudo-second-order model g (mg min)$^{-1}$;

Intra-particle diffusion model:[40]

$$q_t = k_{id} t^{0.5} + C \quad (3)$$

where k_{id} is the rate constant of the intra-particle diffusion model mg (g $min^{0.5})^{-1}$, and C is the intercept of the intra-particle diffusion model (mg g^{-1}).

Table 3 shows the resultant parameters of the experimental data which were fitted to the kinetics models. As described in Table 3, Fig. 6(a)–(c), the kinetics of BPA adsorption on BCs and Cs might be simulated well using a pseudo-second-order kinetics model (correlation coefficients, $R^2 > 0.996$ for BCs and $R^2 > 0.998$ for Cs), indicating a chemisorption process. Additionally, according to the pseudo-second-order model (2), the maximum BPA adsorption capacities of BCs and Cs were 7.199 and 3.860 mg g^{-1}.

To further investigate BPA adsorption by the carbocatalysts, Langmuir (4) and Freundlich (5) adsorption isotherms were used to fit the adsorption equilibrium, as shown in Fig. 6(d)–(f).

Langmuir isotherm model:[41]

$$\frac{C_e}{q_e} = \frac{1}{K_L q_m} + \frac{C_e}{q_m} \quad (4)$$

where C_e is the equilibrium concentration of BPA solution mg L^{-1}, q_m is the maximum adsorption capacity constant for the Langmuir isotherm model in mg g^{-1}, and K_L is the equilibrium adsorption constant for the Langmuir isotherm model in L mg^{-1}.

Freundlich isotherm model:[42]

$$\log q_e = \frac{1}{n}\log C_e + \log K_F \quad (5)$$

where n is the Freundlich adsorption model exponent, K_F is the constant related to the relative sorption capacity of adsorbent in mg g^{-1}.

As shown in Table 4, the Langmuir isotherm equation appeared to be most suitable to describe the adsorption of BPA on BCs and Cs, yielding R^2 values above 0.998 for BCs and 0.993 for Cs. This indicated that the isothermal adsorption behavior of BPA on BCs and Cs followed the Langmuir model and proved that a monolayer adsorption of BPA occurred on homogeneous BCs and Cs surfaces.[43]

3.3.2. Kinetic analysis. The effect that the dosage of BCs and Cs used has on the removal of BPA in the BCs/PS and Cs/PS systems was investigated. The relationship was determined as shown in Fig. S3.† The adsorption rates increased as the BCs and Cs dosages increased from 0.05 to 0.25 g L^{-1}. The BPA removal rate apparently increased due to the addition of PS. Taking BCs as an example (Fig. S3(b)†), when the BCs dosage was 0.05, 0.15, 0.20 and 0.25 g L^{-1}, the BPA adsorption capacities after 60 min were 26.63%, 51.59%, 56.70% and 59.52%, respectively. The simultaneous use of PS and BCs resulted in BPA removal rates that were greatly enhanced to 37.97%, 87.94%, 94.77% and 98.76%, respectively. Previous studies[17,44,45] proved that the heterogeneous catalytic oxidation of dissolved organic compounds can be described by a Langmuir–Hinshelwood (L–H) kinetics model (6),

$$-\frac{dC}{dt} = \frac{kKC}{1+KC} \quad (6)$$

where C (mmol L^{-1}) is the concentration of BPA, K is the equilibrium adsorption constant, and k is the rate constant.

According to previous studies,[17,44,45] eqn (6) can be simplified to eqn (7).

$$C^{1-n} = (n-1)k_{app}t + C_0{}^{1-n} \quad (7)$$

where C_0 (mmol L^{-1}) is the initial BPA concentration, n is the apparent order of the reaction, and k_{app} is the apparent rate constant.

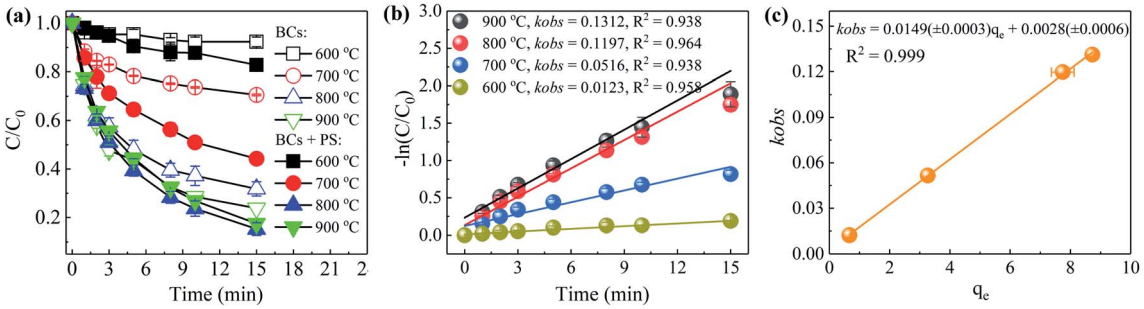

Fig. 5 BPA removal efficiency produced by BCs at different calcination temperatures (a), the associated reaction rates (b), and the correlation of k_{obs} to q_e (c) ($[BPA]_0 = 0.02$ mM, $T = 25 \pm 1$ °C, [BCs] = 0.04 g L^{-1}, $[PS]_0 = 2$ mM, $pH_0 = 4.0 \pm 0.1$).

Table 3 Kinetic parameters for the adsorption of BPA onto BCs and Cs

Adsorption kinetics	Pseudo-first-order		Pseudo-second-order		Intra-particle diffusion		
	k_1 (g mg^{-1} min^{-1})	R^2	k_2 (g mg^{-1} min^{-1})	R^2	k_{id} (mg g^{-1} min$^{-0.5}$)	C (mg g^{-1})	R^2
BCs	0.133	0.735	0.080	0.996	0.276	0.399	0.900
Cs	0.066	0.744	0.170	0.998	0.147	0.204	0.919

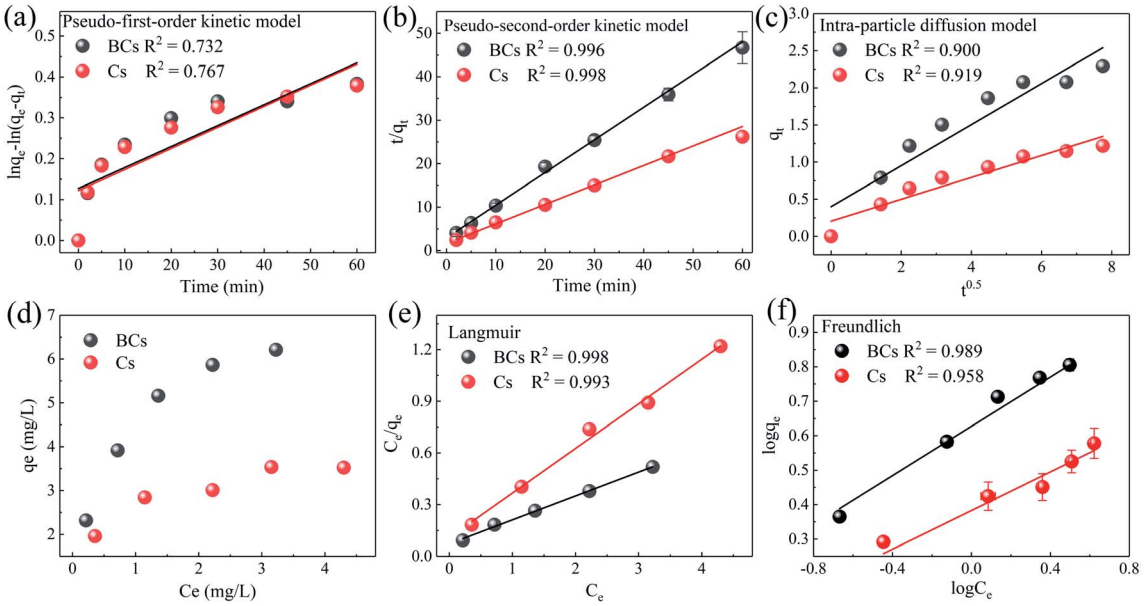

Fig. 6 Plots fitting experimental data to pseudo-first-order (a), pseudo-second-order (b), and intra-particle diffusion (c) models for BPA removal using BCs and Cs. Adsorption isotherms for the adsorption of BPA to BCs and Cs (d) Langmuir fitting (e), and Freundlich fitting (f) ($[BPA]_0$ = 0.02 mM, $T = 25 \pm 1$ °C, $[BCs]_0 = [Cs]_0 = 0.1$ g L^{-1}, $pH_0 = 4.0 \pm 0.1$).

In this work, the BPA degradation kinetics when using the Cs/PS and BCs/PS systems are as shown in Fig. 7. When the carbon material dosages were 0.05, 0.15, 0.20 and 0.25 g L^{-1}, the resulting R^2 values were 0.9785, 0.9963, 0.9962, 0.9938 for Cs and 0.9973, 0.9973, 0.9978, 0.9993 for BCs, respectively. These results demonstrate that the removal of BPA using the Cs/PS and BCs/PS systems fitted eqn (7) well. This indicates that adsorption and oxidation of BPA on Cs and BCs could be theoretically evaluated using the L–H kinetics model and that the boron-modified carbon materials could promote the activation of PS activation for BPA degradation.

3.3.3. Identification of reactive species. Organic contaminant degradation *via* the activation of PS activation using a carbocatalyst has been reported previously and the reactive species generally include singlet oxygen,[8,35] $^{\bullet}OH$, $SO_4^{\bullet-}$,[22] and the reactive electron-deficient carbocatalysts ([carbon]*).[46,47] Ethanol was employed as a typical scavenger for both $SO_4^{\bullet-}$ (k = 1.6–7.7 × 10^7 M^{-1} s^{-1}) and $^{\bullet}OH$ (k = 1.2–2.8 × 10^9 M^{-1} s^{-1}) and in this study, as shown in Fig. 8(a), a negligible effect on the BPA removal was observed when ethanol was added into the PS/BCs system. Fig. 8(b) shows that the EPR signals for DMPO-OH[48] and DMPO-SO_4[49,50] were so weak that they couldn't be detected, indicating that the BPA degradation might proceed *via* a non-radical pathway. Furthermore, the EPR results presented in Fig. 8(c) showed that the PS/BCs/TEMP system resulted in a TEMPN signal intensity that was comparable with that of the PS/TEMP system, demonstrating that singlet oxygen was not the primary reactive species in the non-radical pathway for BPA removal.

3.3.4. Electrochemical analysis. The propensity of a material toward electron donation is closely related to the extent of BPA removal. In our study, in order to investigate the existence of [carbon]*, an electrochemical analysis was applied. We proposed that the BPA removal capacity was influenced by the electron transfer capacity of our material and an electrochemical analysis proved the hypothesis.

CV analysis is widely used to identify the redox potentials of compounds. The CV spectra of BCs and Cs are shown in Fig. 9(a). Ordinarily, there are two pairs of typical oxidation-reduction peaks in CV profiles. The potential of the redox peak for BCs was higher than that for Cs, implying that BCs has a higher current density and more remarkable catalytic activity than Cs.[46] The occurrence of direct electron transfer was also suggested by the Tafel corrosion analysis. The results showed that BCs had a remarkable electron transfer rate for BPA removal because its corrosive potential was lower than that of Cs (Fig. 9(b)).[51]

Table 4 Adsorption isotherm parameters for BPA adsorption onto BCs and Cs

Adsorption isotherm	Langmuir			Freundlich		
	q_e/(mg g^{-1})	K_L/(L mg^{-1})	R^2	K_F/(mg g^{-1})	N	R^2
BCs	7.199	1.913	0.998	4.296	2.667	0.989
Cs	3.860	2.401	0.993	2.580	4.168	0.958

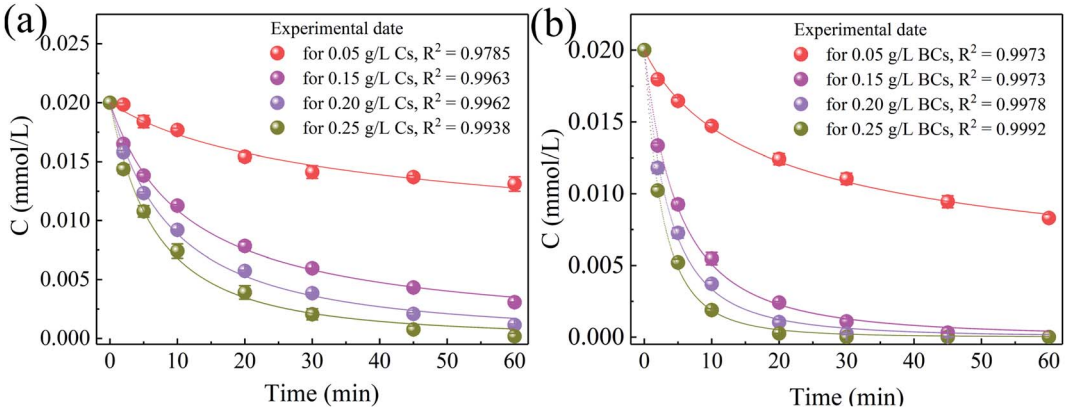

Fig. 7 Kinetic analysis for BPA removal by Cs/PS (a) and BCs/PS (b) ([BPA]$_0$ = 0.02 mM, T = 25 ± 1 °C, [BCs]$_0$ = [Cs]$_0$ = 0.05–0.25 g L^{-1}, [PS]$_0$ = 2 mM, pH$_0$ = 4.0 ± 0.1).

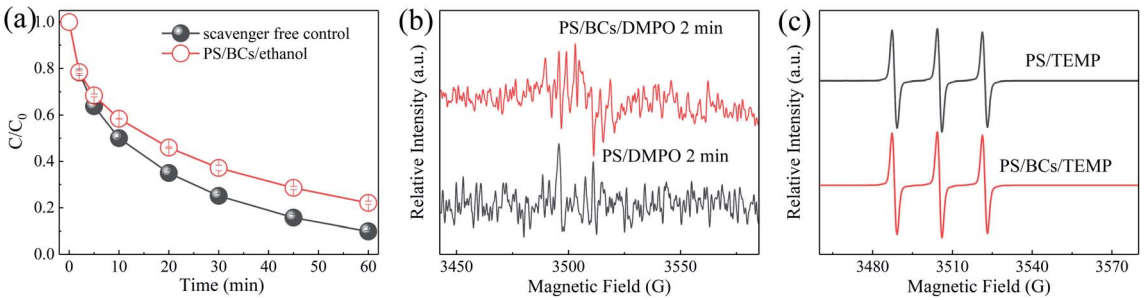

Fig. 8 (a) Quenching test in the PS/BCs system ([BPA]$_0$ = 0.02 mM, T = 25 ± 1 °C, [BCs]$_0$ = 0.1 g L^{-1}, [PS]$_0$ = 1 mM, [ethanol]$_0$ = 100 mM, pH$_0$ = 4.0 ± 0.1); (b) EPR spectra obtained from the PS/BCs systems in aqueous solution ([BCs]$_0$ = 1.0 g L^{-1}, [PS]$_0$ = 10 mM, [DMPO] = 20 mM); and (c) EPR spectra of TEMP-$^1O_2$ adduct (TEMPN) formed in aqueous solutions containing PS, BCs, and TEMP ([BCs]$_0$ = 1 g L^{-1}, [PS]$_0$ = 10 mM, [TEMP] = 20 mM).

The open circuit voltages of Cs (Fig. 9(c)) and BCs (Fig. 9(d)) indicate that BCs had an open circuit voltage of approximately 0.2 V (*vs.* NHE), double that of Cs (approximately 0.1 V). Furthermore, the potential of [carbon]* can also be identified from the equilibrium values of the open circuit voltage. Thus, the open circuit potentials of [BCs]* and [Cs]* were measured to evaluate the electron transfer process. If PS was added into the reaction mixture, the open circuit potential raised sharply and the potential of [BCs]* was raised to around 0.75 V (0.55 V for Cs). In addition, when the BPA was added into the reaction mixture the equilibrium potential rose further. As mentioned previously, in the system where PS is activated by BCs, the potential of the [BCs]* complexes was profoundly elevated, therefore increasing the BPA removal efficiency *via* an electron transfer pathway.

3.3.5. Exploring the role of B in the PS/BCs system. As displayed in Fig. 10(a), the adsorption capacity increased obviously when the amount of B doping increased. In the presence of PS, the BPA removal efficiency was enhanced significantly. When the amount of B doping was 0.7, 1.4, 1.75, and 2.1 g, the BPA removal efficiencies were 57.6%, 79.6%, 85.6%, and 93.5% after 15 min, respectively. Fig. 10(d) indicates that the adsorption efficiency of PS was enhanced more by BCs compared with by Cs. The pseudo-first order kinetics with respect to the level of B doping were found to give relatively good linearity (Fig. 10(c), R^2 = 0.956 and Fig. 10(f), R^2 = 0.986). These results confirmed the important role that the level of B doping plays as it not only increased the BPA adsorption rate, but also the PS adsorption quantity. This result indicates that the introduction of B into

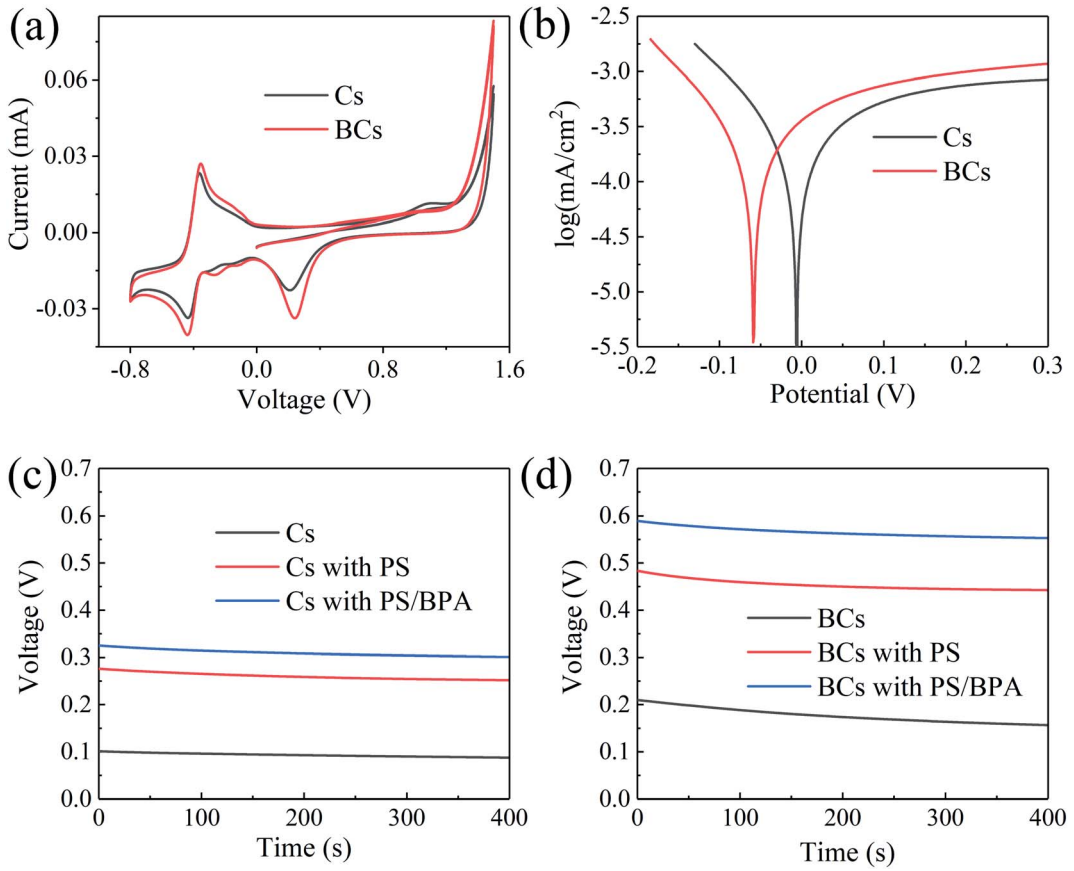

Fig. 9 CV curves of Cs and BCs obtained at the scan rate of 10 mV s^{-1} (a); Tafel corrosion scan curves for Cs and BCs (b); and open circuit voltages of Cs (c) and BCs (d) (glassy carbon electrodes, $[BPA]_0 = 0.10$ mM, $T = 25 \pm 1$ °C, $[PS]_0 = 1.00$ mM).

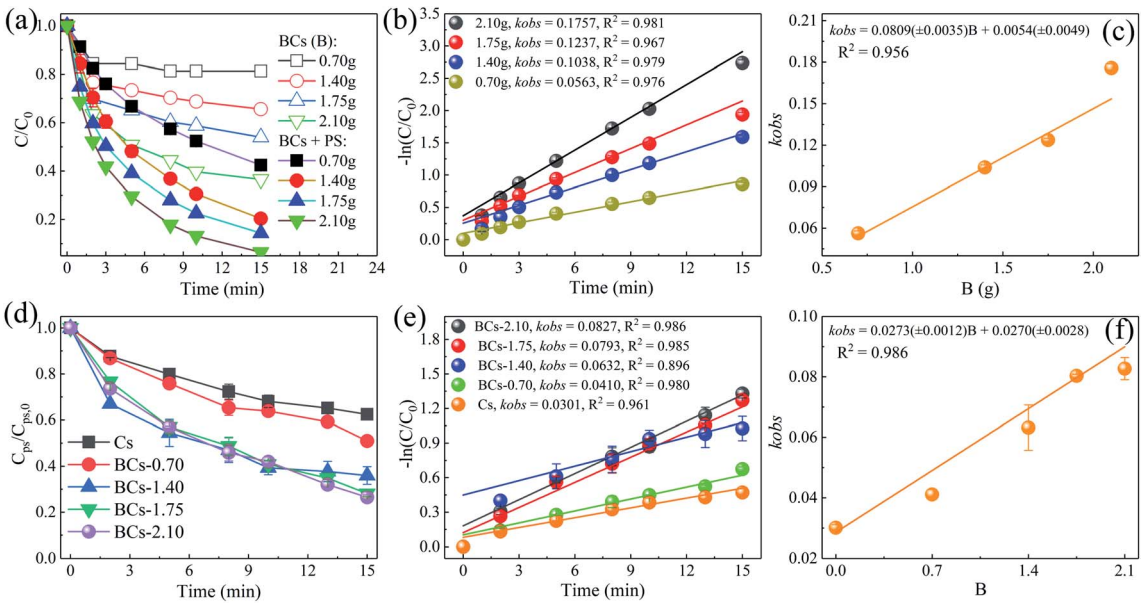

Fig. 10 Effect of different B doping levels on BPA removal in the PS/BCs systems (a); the associated reaction rates (b); and the correlation of k_{obs} to the level of B doping (c) ($[BPA]_0 = 0.02$ mM, $T = 25 \pm 1$ °C, $[BCs] = 0.04$ g L^{-1}, $[PS]_0 = 2$ mM, $pH_0 = 4.0 \pm 0.1$). Effect of different B doping levels on PS adsorption without BPA in the PS/BCs systems (d); the associated reaction rates (e); and the correlation of k_{obs} to the level of B doping (f) ($T = 25 \pm 1$ °C, $[BCs] = 0.04$ g L^{-1}, $[PS]_0 = 2$ mM, $pH_0 = 4.0 \pm 0.1$).

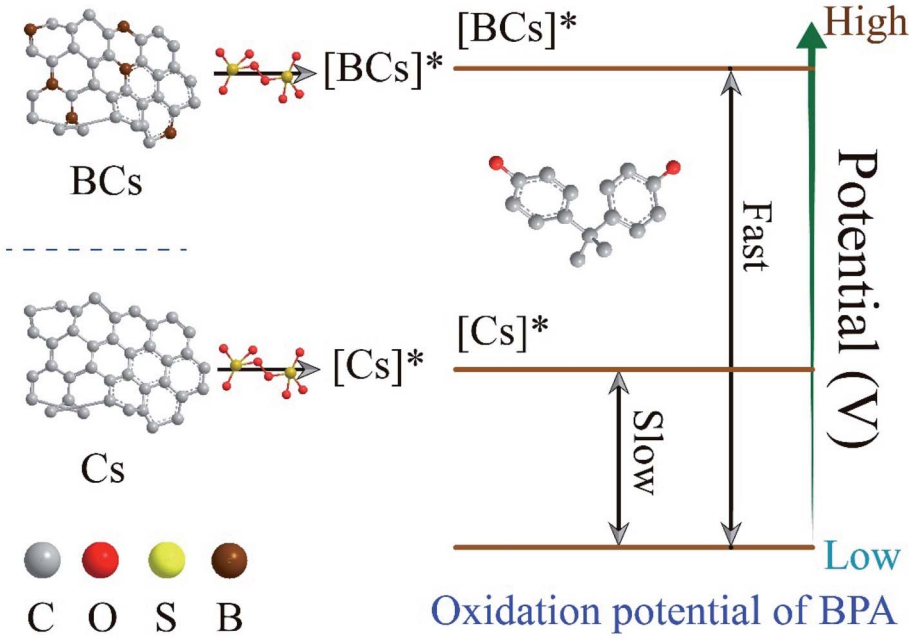

Scheme 1 Proposed mechanism for the degradation of BPA.

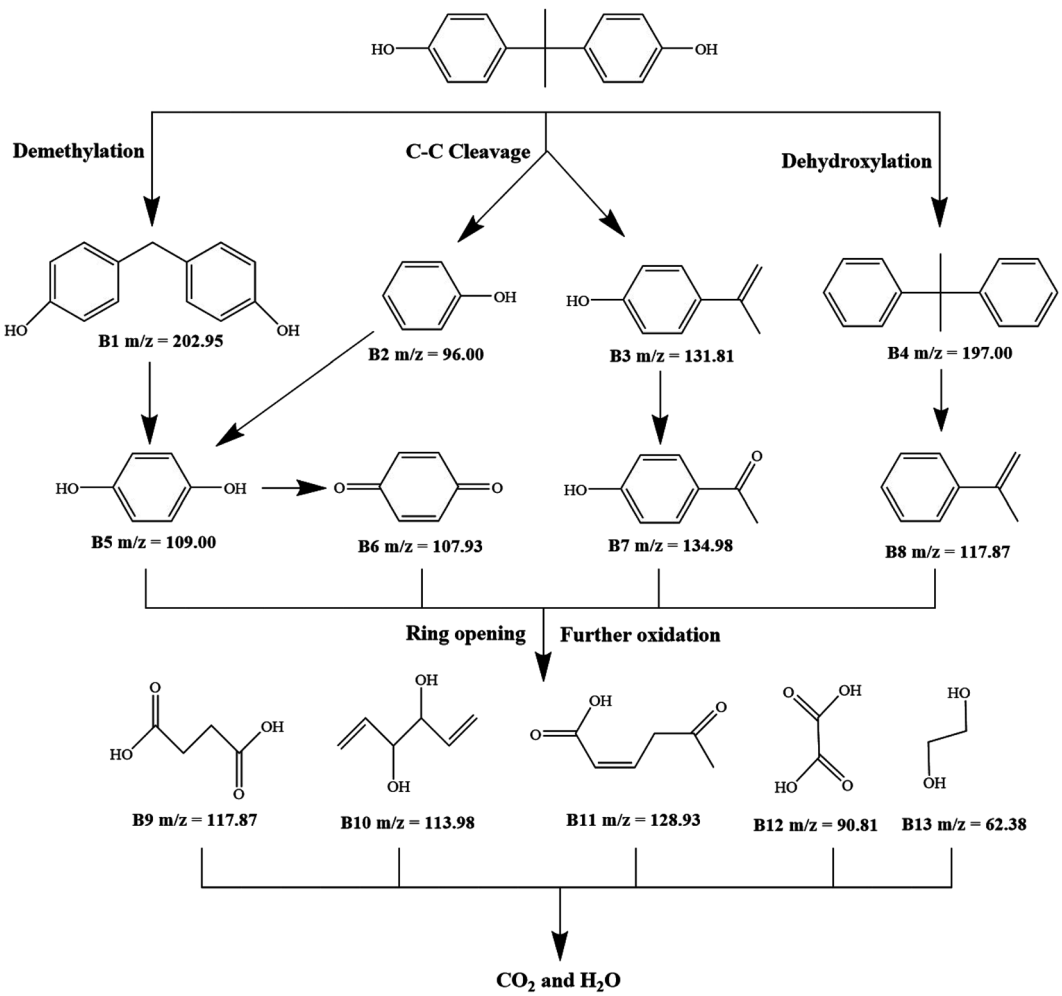

Fig. 11 Potential BPA degradation pathways.

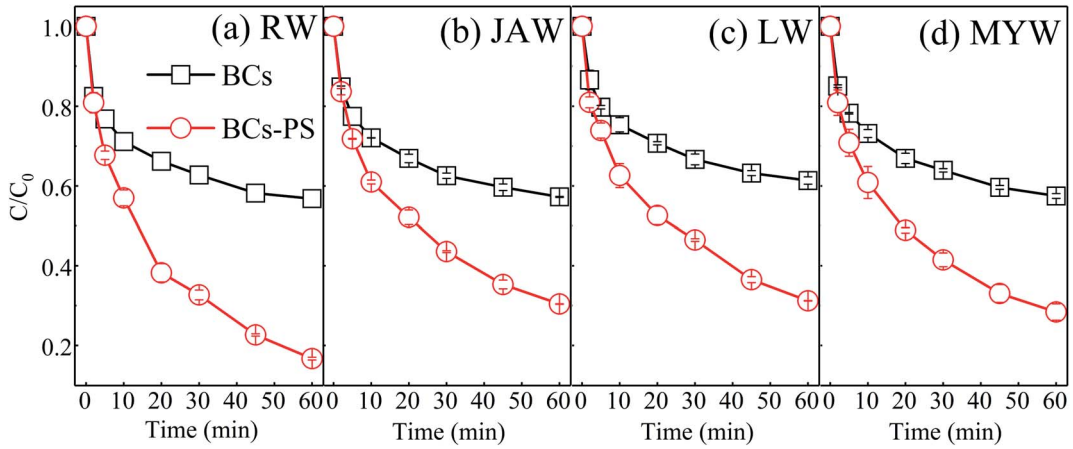

Fig. 12 BPA removal in simulated wastewaters ($[BPA]_0$ = 0.02 mM, T = 25 ± 1 °C, $[BCs]_0 = [Cs]_0$ = 0.1 g L^{-1}, $[PS]_0$ = 2 mM, pH_0 = 4.0 ± 0.1).

carbon material clearly enhanced the catalytic activities of the carbon catalysts.

Based on the above discussions, we proposed a nonradical mechanism, as depicted in Scheme 1. (i) The unpaired electrons on BCs are removed by PS and subsequently form a metastable intermediate, [BCs]*, which could increase the redox potential of BCs; (ii) [BCs]* fills the newly created vacancies by capturing electrons from BPA, thus oxidizing BPA; and (iii) in certain circumstances, when the quantity of B doping is increased, the potential of the [BCs]* complex becomes more positive, giving it a higher oxidation capacity and accelerating the electron transfer from BPA, thus boosting the BPA removal rate.

3.4. Possible BPA degradation pathways

The intermediate products generated after 30 min of BPA degradation were identified using liquid chromatography with mass spectrometry (LC-MS). Various intermediates were detected, and the possible intermediate products are proposed in Table S1.†[2,52–57] Three possible oxidative pathways for the degradation of BPA are proposed. As displayed in Fig. 11, in pathway I, BPA is directly changed into two intermediates m/z 96.00 (B2, phenol) and m/z 131.81 (B3, 4-vinylphenol) *via* a C–C cleavage process. These intermediates are further oxidized into B5 (hydroquinone, m/z = 109.00) and B7 (4-hydroxyacetophenone, m/z = 134.98), respectively. For pathway II, the BCs-PS system could involve demethylation to generate B1 (4-[4-(hydroxymethyl)phenyl] phenol, m/z = 202.95). In subsequent steps, B1 is further decomposed to B5, which could be gradually oxidized to B6 (*p*-benzoquinone, m/z = 107.93). The third pathway is led by a dehydroxylation reaction, where the intermediate B4 (2,2-bis(phenyl)propane, m/z = 197.00) is formed from BPA. This is then converted to B8 (1-methylethenylbenzene, m/z = 117.87) *via* a further oxidation process. In addition, these intermediates would then be degraded by further oxidation and ring opening process. Five peaks with m/z values 117.87 (succinic acid), 113.98 (divinyloxyethane), 128.93 (5-oxohex-2-enoic acid (OEA)), 90.81 (ethanedioic acid) and 62.38 (ethylene glycol) are derived from intermediates B5, B6, B7 and B8. The five smaller intermediates can be finally mineralized into CO_2 and H_2O.

3.5. Impacts of water matrices

The composition of waste water could limit the effectiveness of the BCs/PS system, especially because of the dissolved inorganic ions or particulates.[58,59] Therefore, the effects of different water matrices on BPA removal were also investigated to estimate the interactions between the BCs/PS system and different water matrices, including deionized water (DW), running water (RW), landscape water (LW), Mingyuan lake water (MYW), and Jiang'an river water (JAW). Table S2† displays the characteristics of four actual water samples. The BPA removal efficiency in the DW, RW, JAW, LW and MYW samples were 49.50%, 43.20%, 42.76%, 38.65% and 42.53%, respectively. As shown in Fig. 12, in the presence of PS, the BPA removal efficiencies were respectively 83.29%, 69.59%, 68.78% and 71.60% in RW, JAW, LW and MYW, profoundly lower than in DW (94.15%). This is because the presence of dissolved organic matter and inorganic species could compete with the PS for the reaction sites on the surface of BCs where [BCs]* is produced. This process could also limit the effective adsorption of BPA on the BCs surface, consequently causing a decrease in the removal rate.

4. Conclusions

In this work, B-doped carbocatalysts were prepared for the activation of persulfate (PS) for micropollutant degradation. The results demonstrate that B-doped carbon materials have, when compared with B-free carbon materials, enhanced adsorption and catalytic activity for bisphenol A (BPA) removal. The adsorption process plays a critical role in the subsequent degradation process and the quantity of B doping was identified as the primary factor to attain a greater adsorption quantity of PS and a faster BPA adsorption rate. An electrochemical analysis (cyclic voltammetry, Tafel corrosion analysis and open circuit voltages) proved that boron-doped carbon materials (BCs) could elevate the potential of the derived nonradical [BCs]* complexes, and that an electron transfer pathway for BPA

removal was enhanced *via* the higher potential [BCs]* complexes. This discovery is critical as it reveals the importance of B-doping in carbon materials/PS systems for the removal of BPA *via* nonradical pathways. Moreover, the outstanding performance of B-doped carbon materials means that metal-free catalysis for PS activation can be utilized as an environmentally friendly process for micropollutant reduction.

Conflicts of interest

The authors declare that there are no conflicts of interest.

Acknowledgements

The authors thank Mr Fanghao Liao and Miss Jiayi Yang from Southwest Branch of China Construction Third Engineering Bureau Group Co., Ltd. for help in data analysis.

References

1 G. Ozyildiz, T. Olmez-Hanci and I. Arslan-Alaton, *Appl. Catal., B*, 2019, **254**, 135–144.
2 F. Wang, Y. Lai, Q. Fang, Z. Li, P. Ou, P. Wu, Y. Duan, Z. Chen, S. Li and Y. Zhang, *Appl. Catal., B*, 2020, **262**, 118099.
3 Y. Zhang, D. Zhang, L. Zhou, Y. Zhao, J. Chen, Z. Chen and F. Wang, *Chem. Eng. J.*, 2018, **336**, 690–700.
4 N. Bolong, A. F. Ismail, M. R. Salim and T. Matsuura, *Desalination*, 2009, **239**, 229–246.
5 P. Wu, Y. Zhang, Z. Chen, Y. Duan and S. Li, *Appl. Catal., B*, 2019, **255**, 117784.
6 Y. Shao, L. Zhou, Q. Wu, C. Bao and M. Liu, *J. Hazard. Mater.*, 2017, **339**, 418–426.
7 Z. Peng, Z. Jing, Y. Zhang, G. Zhang, W. Li, C. Wei, J. Liang, Y. Liu and S. Shu, *J. Hazard. Mater.*, 2017, **344**, 1209–1219.
8 X. Huo, P. Zhou, J. Zhang, Y. Liu, X. Cheng, Y. Liu, W. Li and Y. Zhang, *J. Hazard. Mater.*, 2020, **391**, 122055.
9 Y. Fan, Y. Ji, D. Kong, J. Lu and Q. Zhou, *J. Hazard. Mater.*, 2015, **300**, 39–47.
10 R. Yin, W. Guo, H. Wang, J. Du, X. Zhou, Q. Wu, H. Zheng, J. Chang and N. Ren, *Chem. Eng. J.*, 2018, **335**, 145–153.
11 Q. Chengdu, L. Xitao, M. Jun, L. Chunye and X. Li, *Chemosphere*, 2016, **151**, 280–288.
12 F. Rehman, M. Sayed, J. A. Khan, N. S. Shah, H. M. Khan and D. D. Dionysiou, *J. Hazard. Mater.*, 2018, **357**, 506–514.
13 F. Ghanbari and M. Moradi, *Chem. Eng. J.*, 2017, **310**, 41–62.
14 H. Sun, S. Liu, G. Zhou, H. M. Ang, M. Tadé and S. Wang, *ACS Appl. Mater. Interfaces*, 2012, **4**, 5466.
15 H. Sun, Y. Wang, S. Liu, L. Ge, L. Wang, Z. Zhu and S. Wang, *Chem. Commun.*, 2013, **49**, 9914–9916.
16 X. Cheng, H. Guo, Y. Zhang, G. V. Korshin and B. Yang, *Water Res.*, 2019, **157**, 406–414.
17 X. Cheng, H. Guo, Y. Zhang, X. Wu and Y. Liu, *Water Res.*, 2017, **113**, 80–88.
18 K. A. Lin, J. T. Lin, X. Y. Lu, C. Hung and Y. F. Lin, *J. Colloid Interface Sci.*, 2017, **505**, 728–735.
19 X. Duan, Z. Ao, D. Li, H. Sun, L. Zhou, A. Suvorova, M. Saunders, G. Wang and S. Wang, *Carbon*, 2016, **103**, 404–411.
20 H. Lee, H. I. Kim, S. Weon, W. Choi, Y. S. Hwang, J. Seo, C. Lee and J. H. Kim, *Environ. Sci. Technol.*, 2016, **50**, 10134.
21 W. Tian, H. Zhang, X. Duan, H. Sun, M. O. Tade, H. M. Ang and S. Wang, *ACS Appl. Mater. Interfaces*, 2016, **8**, 7184–7193.
22 X. Duan, H. Sun and S. Wang, *Acc. Chem. Res.*, 2018, **51**, 678–687.
23 W. Tian, H. Zhang, H. Sun, M. O. Tadé and S. Wang, *Chem. Eng. J.*, 2018, **347**, 432–439.
24 W. Yu, Y. Feng, X. Liu, G. Tan and X. Dan, *Appl. Surf. Sci.*, 2018, **435**, 281–289.
25 C. Chokradjaroen, S. Kato, K. Fujiwara, H. Watanabe, T. Ishii and T. Ishizaki, *Sustainable Energy Fuels*, 2020, **4**, 4570–4580.
26 S. S. Balaji, P. A. Ganesh, M. Moorthy and M. Sathish, *Bull. Mater. Sci.*, 2020, **43**, 151.
27 S. Kaipannan, P. A. Ganesh, K. Manickavasakam, S. Sundaramoorthy and S. Marappan, *J. Energy Storage*, 2020, **32**, 101774.
28 A. Xk, A. Gf, A. Fs, A. Xd, W. A. Lei, A. Xzf and B. Jlila, *Int. J. Hydrogen Energy*, 2021, **4**, 36221–36231.
29 L. Yang, S. Jiang, Y. Zhao, L. Zhu, S. Chen, X. Wang, Q. Wu, J. Ma, Y. Ma and Z. Hu, *Angew. Chem., Int. Ed.*, 2011, **50**, 7132–7135.
30 L. Yang, S. Jiang, Y. Zhao, L. Zhu, S. Chen, X. Wang, Q. Wu, J. Ma, Y. Ma and Z. Hu, *Angew. Chem., Int. Ed. Engl.*, 2011, **50**, 7132–7135.
31 Y. Xie, Z. Meng, T. Cai and W. Q. Han, *ACS Appl. Mater. Interfaces*, 2015, **7**, 25202–25210.
32 J. Kang, X. Duan, C. Wang, H. Sun, X. Tan, M. O. Tade and S. Wang, *Chem. Eng. J.*, 2018, **332**, 398–408.
33 Y. Liu, W. Li, P. Wu, C. Ma, X. Wu, M. Xu, S. Luo, Z. Xu and S. Liu, *Sens. Actuators, B*, 2019, **281**, 34–43.
34 P. Zhou, W. Ren, G. Nie, X. Li, X. Duan, Y. Zhang and S. Wang, *Angew. Chem., Int. Ed. Engl.*, 2020, **59**, 16517–16526.
35 X. Cheng, H. Guo, Y. Zhang, Y. Liu, H. Liu and Y. Yang, *J. Colloid Interface Sci.*, 2016, **469**, 277–286.
36 W. Tian, H. Zhang, X. Duan, H. Sun, M. O. Tade, H. M. Ang and S. Wang, *ACS Appl. Mater. Interfaces*, 2016, **8**, 7184.
37 S. Zhu, X. Huang, F. Ma, L. Wang and X. Duan, *Environ. Sci. Technol.*, 2018, **52**, 8649–8658.
38 X. Wang, Y. Qin, L. Zhu and H. Tang, *Environ. Sci. Technol.*, 2015, **49**, 6855–6864.
39 Y. Lee, J. Kim and H. Shin, *Sep. Sci. Technol.*, 2013, **48**, 1093–1101.
40 F. Zhang, J. Lan, Y. Yang, T. Wei, R. Tan and W. Song, *J. Nanopart. Res.*, 2013, **15**, 1–10.
41 Y. Shao, X. Wang, Y. Kang, Y. Shu, Q. Sun and L. Li, *Acta Sci. Circumstantiae*, 2014, **429**, 25–33.
42 S. H. Huo and X. P. Yan, *J. Mater. Chem.*, 2012, **22**, 7449–7455.
43 D. P. Li, Y. R. Zhang, X. X. Zhao and B. X. Zhao, *Chem. Eng. J.*, 2013, **232**, 425–433.
44 N. G. Asenjo, R. Santamaría, C. Blanco, M. Granda, P. álvarez and R. Menéndez, *Carbon*, 2013, **55**, 62–69.

45 L. Li, L. Gong, Y. X. Wang, Q. Liu, J. Zhang, Y. Mu and H. Q. Yu, *Water Res.*, 2016, **98**, 235–241.
46 W. Ren, L. Xiong, X. Yuan, Z. Yu and S. Wang, *Environ. Sci. Technol.*, 2019, **53**, 14595–14603.
47 W. Ren, L. Xiong, G. Nie, H. Zhang and S. Wang, *Environ. Sci. Technol.*, 2019, **54**, 1267–1275.
48 P. Guilong, M. Zhang, S. Deng, D. Shan and H. Qiang, *Chem. Eng. J.*, 2018, **341**, 361–370.
49 P. Zhou, W. Li, J. Zhang, G. Zhang, X. Cheng, Y. Liu, X. Huo and Y. Zhang, *J. Taiwan Inst. Chem. Eng.*, 2019, **100**, 202–209.
50 P. Zhou, J. Zhang, Z. Xiong, Y. Liu and Y. Zhang, *Appl. Catal., B*, 2019, **265**, 118264.
51 M. Zhao, C. Zhang, X. Yang, L. Liu, X. Wang, W. Yin, Y. Li, S. Wang and W. Fu, *J. Hazard. Mater.*, 2020, **396**, 122712.
52 A. Bacha, I. Nabi, H. Cheng, K. Li, S. Ajmal, T. Wang and L. Zhang, *Chem. Eng. J.*, 2020, **389**, 124482.
53 X. Dong, B. Ren, Z. Sun, C. Li, X. Zhang, M. Kong, S. Zheng and D. D. Dionysiou, *Appl. Catal., B*, 2019, **253**, 206–217.
54 S. Wang, J. Tian, Q. Wang, F. Xiao and F. Cui, *Appl. Catal., B*, 2019, **256**, 117783.
55 L. Yang, X. Bai, J. Shi, X. Du and P. Jin, *Appl. Catal., B*, 2019, **256**, 117759.
56 X. Zhang, R. Zhao, N. Zhang, Y. Su and C. Du, *Appl. Catal., B*, 2019, **263**, 118316.
57 J. Lin, Y. Hu, L. Wang, D. Liang and S. Shao, *Chem. Eng. J.*, 2019, **382**, 122931.
58 E. Díez-Mato, F. C. Cortezón-Tamarit, S. Bogialli, D. García-Fresnadillo and M. D. Marazuela, *Appl. Catal., B*, 2014, **160–161**, 445–455.
59 L. Hu, G. Zhang, M. Liu, Q. Wang and P. Wang, *Chem. Eng. J.*, 2018, **338**, 300–310.